2013 European Control Conference (ECC)
July 17-19, 2013, Zürich, Switzerland.

Resonance-shifting Integral Resonant Control Scheme for Increasing the Positioning Bandwidth of Nanopositioners

Mohammad Namavar, *Student Member, IEEE*, Andrew J. Fleming, *Member, IEEE*, and Sumeet S. Aphale, *Member, IEEE*

***Abstract*— The performance of precision mechatronic systems is restricted by their first dominant resonant mode. Damping techniques have be employed to suppress this resonance peak and improve the performance. To increase the bandwidth of the system feed-forward techniques have been used but they can be very sensitive to modeling errors as well as loading effects. In this paper a simple frequency shifting controller is introduced and is combined with Integral Resonant Control (IRC). Using these controllers can increase the bandwidth of the system to a desired amount. Systems with colocated sensor-actuator pairs exhibit the interesting property of pole-zero interlacing. IRC exploits this property by changing the pole-zero interlacing to zero-pole interlacing. The unique phase response of this class of systems enables a simple integral feedback controller to add substantial damping.**

I. Introduction

Unwanted excitation of system resonances produce vibration that can substantially degrade the performance and life time of many mechatronic systems [1]. Damping these vibrations has been a key research focus which has led to innovations in a multitude of areas such as structural design, novel materials, and control [1]. Yet, unwanted vibrations are a part of many technological systems and continue to motivate research in vibration control. Both passive and active damping techniques have been widely reported in the literature. Passive damping techniques have the advantage of needing no sensing or supervisory control but can be limited in performance and may be sensitive to changes in system resonance frequency. Active techniques may be more complicated but have the potential to overcome the performance limitations of passive systems [2].

Current damping controllers include Positive Position Feedback [3], Positive Velocity and Position Feedback [4], resonant control [5], and robust control [6]. A drawback of many present control techniques is the high-order controller required to control a system with multiple resonances. To avoid this difficulty, Integral Resonant Control (IRC) was proposed as a simple, low-order scheme capable of damping multiple modes while retaining high stability margins [7].

In this work we are interested to study the nanopositioning systems as our system. Damping techniques for these positioners are applied successfully to suppress the resonance peak but their performance still is limited by the the maximum bandwidth of the system. To overcome the bandwidth limitations, researchers currently design new mechanical platforms [8]. In this work a modified control scheme is introduced, which increases the bandwidth of interest well beyond the initial bandwidth.

M. Namavar and S. S. Aphale are with the Center for Applied Dynamics Research, School of Engineering, University of Aberdeen, UK.

A. J. Fleming is with the Center for Complex Dynamic Systems and Control, School of Electrical Engineering and Computer Science, University of Newcastle, Australia

A. Overview

In section II, a fourth order model (for two resonant modes) is identified to match the measured frequency response of one axis of a commercially available nanopositioning platform. A detailed analysis of the resonance-shifting method is presented. Section III describes how the resonance-shifting technique and IRC technique results in a substantial increase in the overall positioning bandwidth. Section IV presents simulation results along with a performance comparison of the modified controller with standard IRC. VI concludes the paper.

II. System Modeling

Piezoelectric nanopositioning systems are either tube-type or stack-actuated platforms. In both cases, the system frequency response functions (FRF) exhibit a dominant lightly damped resonance mode and can be modeled as a second order system. Transfer functions of these systems are of the form (1), where ζ is the damping coefficient and ω_p is the resonance frequency. To compensate for the truncation-induced modeling error, a small and positive feed-through term d is usually introduced [9].

$$G(s) = \frac{\sigma^2}{s^2 + 2\zeta\omega_p s + \omega_p^2} + d. \tag{1}$$

Throughout this paper, a second order model (2) of the nanopositioning platform reported in [10] is used.

$$\hat{G(s)} = \frac{8.3782 \times 10^6}{s^2 + 57.2s + 6.657 \times 10^6}. \tag{2}$$

A detailed fourth-order model which includes the higher order colocated dynamics is given by (3):

$$G(s) = \frac{8.3782 \times 10^6 s^2 + 2.1161 \times 10^8 s + 1.05 \times 10^{14}}{s^4 + 114s^3 + 1.926 \times 10^7 s^2 + 1.2 \times 10^9 s + 8.39 \times 10^{13}}. \tag{3}$$

Fig. (1) plots the measured FRF, the fourth-order model magnitude plot, and the pole-zero map of the model which shows pole-zero interlacing.

In this paper, a three step control design is introduced as follow:

- Resonance-shift Controller, which is a negative unity feedback loop

- Damping Controller, which employs the IRC technique in positive feedback loop
- Tracking Controller, which is an integral controller implemented in negative feedback loop

Each step is discussed in detail in the following section.

III. Controller Design

Step1: Resonance shifting - Usually a triangle wave and a ramp signal are used to create a raster pattern that the nanopositioner follows. The triangle wave is a high-bandwidth signal consisting of (ideally infinite) odd harmonics of its fundamental frequency. The achievable positioning bandwidth is limited by the resonance frequency of the platform axis and quite often, the fundamental frequency is chosen to be $1/100^{th}$ of the platform resonance. The resonance-shifting controller is introduced to overcome this constraint. This controller is basically a negative proportional feedback loop Fig. 2(a).

This controller not only shifts the resonance peak but also increases the maximum peak value (by reducing ζ). This negative feedback loop is always stable for a second order system and by increasing the gain $\hat{k}$ the DC gain of the loop approaches unity. This is shown below where H_1 is the transfer function for the resonance-shifted closed-loop system:

$$\begin{aligned} \hat{G} &= \frac{\sigma^2}{s^2+2\zeta\omega_p s+\omega_p^2} \\ H_1 &= \frac{\hat{k}G}{1+\hat{k}G} \\ H_1 &= \frac{\hat{k}\sigma^2}{s^2+2\zeta\omega_p s+\omega_p^2+\hat{k}\sigma^2} \end{aligned} \tag{4}$$

Henceforth, the system subjected to damping and tracking controller is given by:

$$H_1(s) = \frac{\bar{\sigma}^2}{s^2+2\bar{\zeta}\bar{\omega}_p s+\bar{\omega}_p^2}$$

where $\bar{\sigma}^2=\hat{k}\sigma^2$ and $\bar{\omega}_p^2=\omega_p^2+\hat{k}\sigma^2$.

By comparing the platform transfer function and H_1, relationships between $\bar{\zeta}$ and other parameters can be identified:

$$\begin{aligned} 2\bar{\zeta}\bar{\omega}_p &= 2\zeta\omega_p \\ \Rightarrow \frac{\bar{\zeta}}{\zeta} &= \frac{\omega_p}{\bar{\omega}_p} \end{aligned} \tag{5}$$

Equation (5) shows that increasing resonance frequency by a factor of α will reduce the damping ratio by $1/\alpha$. In most closed-loop second-order system analysis, the damping ratio is usually neglected for sake of simplicity. The same simplification will be applied to all the analysis presented in the work that follows. As we have further reduced the damping coefficient, this simplification is more valid. The DC gain of H_1 is $\hat{k}\sigma^2/(\omega_p^2+\hat{k}\sigma^2)$. Since for most of the systems σ^2 and ω_p^2 are almost equal, the DC gain can be estimated as:

$$DC_{gain} \approx \frac{\hat{k}\omega_p^2}{(\hat{k}+1)\omega_p^2} \approx 1 = 0dB$$

1) Relation between sensor bandwidth and $\hat{k}$: Sensor bandwidth is one of the limiting factors for the amount of resonance shift. The shifted resonance should be within the sensor bandwidth γ. Considering shifted resonance frequency be $(\omega_p^2+\hat{k}\sigma^2)^{1/2}$, then:

$$\begin{aligned} (\omega_p^2+\hat{k}\sigma^2)^{1/2} &< \gamma \\ \hat{k} &< \frac{\gamma^2-\omega_p^2}{\sigma^2} \end{aligned} \tag{6}$$

Step 2: Damping Controller - The general concept of the IRC design can summarized below:

Given that a colocated system $G(s)$ with pole-zero interlacing is to be damped, an adequate feed-through term 'd' can first be added to the system to reverse the interlacing from pole-zero to zero-pole. Furthermore, if a simple integrator $C(s)=\frac{k}{s}$ is implemented in positive feedback with such a modified system $\hat{G}(s)=G(s)+d$, as the integral gain 'k' is increased, the poles of the system traverse a curve where first they move away from the imaginary axis, into the left-half complex plane (thus increasing their damping coefficient) and then back towards the imaginary axis till they reach their correspondingly paired zero (with reduced damping).

2) Relationship between feed-through, damping and IRC gain: In [11], a full mathematical derivation of the relationship between feed-through, damping and IRC gain has been presented. The main results are summarized below.

Theorem 1: Consider a colocated system with a pair of complex poles at $\pm j\omega_p$ and feed-through induced zeros at $j\omega_z > j\omega_p/3$. If the IRC strategy is implemented, the maximum damping achievable is given by

$$\zeta_{max}=\frac{1}{2}\left(\frac{\omega_p}{\sqrt{\omega_p^2+\sigma^2/d}}-1\right). \tag{7}$$

The controller gain required to reach this maximum damping is given by

$$k=\frac{1}{|d|}\left(\omega_p\sqrt{\frac{\omega_p}{\sqrt{\omega_p^2+\sigma^2/d}}}\right), \tag{8}$$

where $\omega_z=\sqrt{\omega_p^2+\sigma^2/d}$ with respect to d.

Step 3: Tracking controller - The IRC algorithm has been applied to damp the resonances of various precision positioning systems, especially nanopositioners [12]–[16]. Nanopositioning systems generally employ piezoelectric actuators that tend to introduce nonlinear effects such as hysteresis and creep. To minimize the positioning errors introduced by these phenomena, a damping controller such as IRC is used in conjunction with a simple integral tracking scheme [10], [17]. A block diagram of the typical control scheme

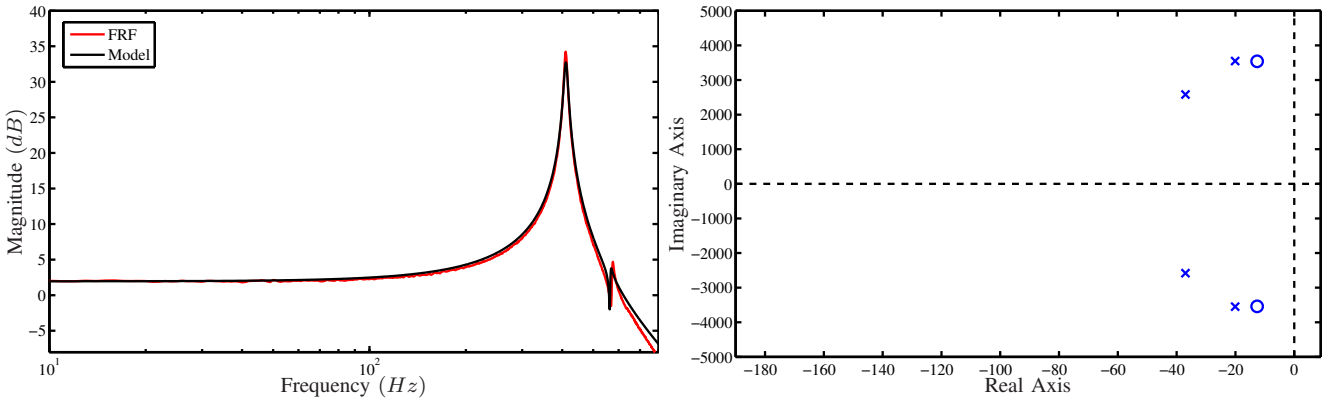

(a) (b)

Fig. 1. (a) shows the measured FRF and the fourth-order model magnitude plot. The identified model is sufficiently accurate with respect to measured data. (b) The pole-zero map shows that the system exhibits pole-zero interlacing.

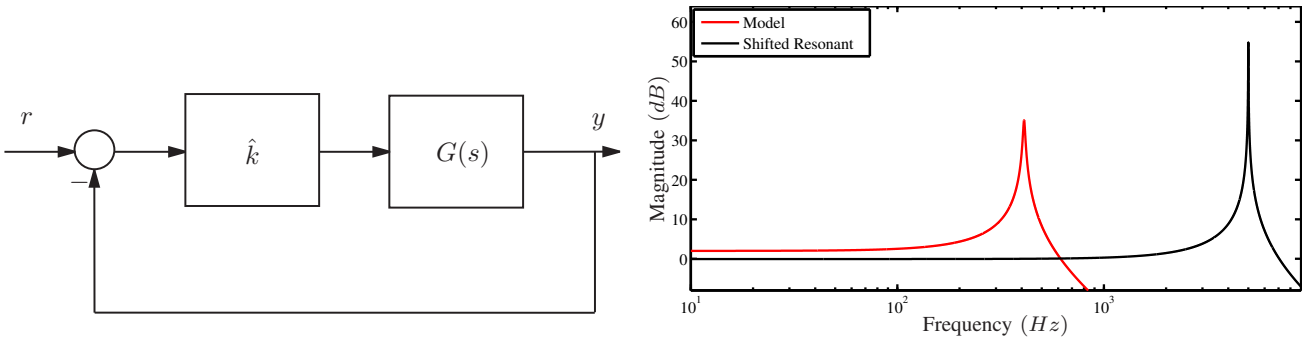

(a) (b)

Fig. 2. (a) Block diagram of the Resonance-shifting controller. This controller consist of a gain implemented in a negative unity feedback. (b) Magnitude response of the original system and the resonance-shifted system.

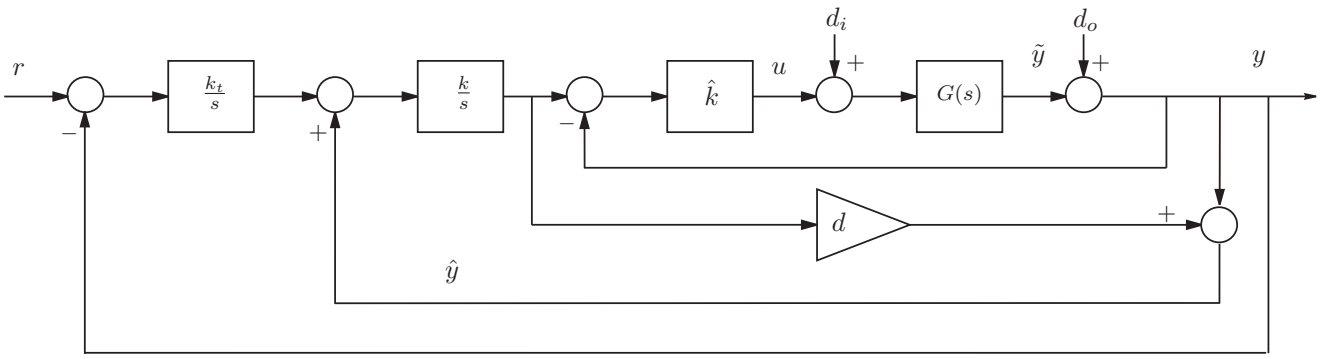

Fig. 3. (a) Block diagram for the Resonance-shifting controller, IRC damping controller and Integral tracking controller scheme where d is the feed-through term, $\hat{k}$ is the resonance shifting gain, k is the IRC damping gain and k_t is the integral tracking gain.

incorporating both IRC damping and integral tracking along with the resonance-shifting controller is shown in Fig. (3).

In Fig. (3), the transfer functions of interest for quantification of positioning performance are y/r (output to input) and y/d_i (output to input disturbance). To find the characteristic equation $C(s)$, four loops L_1, L_2, L_3 and L_4 are defined as below:

$$\begin{aligned} L_1 &= -\hat{k} \times G(s) \\ L_2 &= \frac{k}{s} \times \hat{k} \times G(s) \\ L_3 &= \frac{k}{s} \times d \\ L_4 &= -\frac{k_t}{s} \times \frac{k}{s} \times \hat{k} \times G(s). \end{aligned}$$

Using Mason's rule, $C(s)$ is the numerator of (9).

$$1 - (L_1 + L_2 + L_3 + L_4) + (L_1 L_3) \tag{9}$$

Roots of the denominator of (9) are zeros of different transfer functions or they may cancel out. But the zeros of (9) are the poles of the final closed-loop transfer function. Stability of the closed-loop transfer function is the most important factor in any control application. H_1 as defined before, can be considered as the new system which needs to be damped and tracked. Hence, the relationship between damping and tracking controller can be defined by *Theorem 2* [11].

Theorem 2: Let k and k_t be the IRC damping and integral tracking gains respectively. Then, for the closed-loop system as implemented in Fig. (3) to be stable, the gains must obey the following inequality:

$$k_t k < -\frac{\bar{\sigma}^2 + d\bar{\omega}_p^2}{d^2} \tag{10}$$

This theorem proves that damping and tracking gains are related in the IRC scheme and cannot be arbitrarily tuned independent of each other.

Corollary 3: For a given second order system controlled using the scheme shown in Fig. (3), there exists an absolute maximum value for $k_t k$. The corresponding maximum value is related to d by:

$$d = -2\frac{\bar{\sigma}^2}{\bar{\omega}_p^2} = 2d_c \tag{11}$$

$$\max\{k_t k\} = \frac{\bar{\omega}_p^4}{4\bar{\sigma}^2} \tag{12}$$

IV. Simulation and Results

For simulations presented here, the FRF measured for one axis of the PI-734 XY nanopositioning platform [10] was used. This platform has a dominant resonant mode at $411\ Hz$ and shows pole-zero interlacing for higher frequencies, making it an appropriate choice for the IRC scheme. The modeled transfer function is:

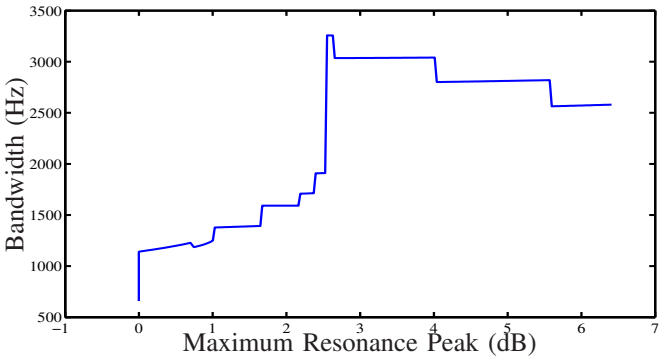

Fig. 4. Numerical evaluation of bandwidth of the overall controlled system is plotted against the maximum resonance peak, for different tracking gains, while resonance shifting and damping gains are fixed. Here, the bandwidth is defined as a range of frequencies where DC gain of the system lies between ± 1 dB. Maximum achievable bandwidth is 3260 Hz which is achieved by $k_t = 7640$.

$$G(s) = \frac{8.3782 \times 10^6 s^2 + 2.1161 \times 10^8 s + 1.05 \times 10^{14}}{s^4 + 114s^3 + 1.926 \times 10^7 s^2 + 1.2 \times 10^9 s + 8.39 \times 10^{13}}. \tag{13}$$

To design the controllers, we considered the simpler second order model which matches the dominant mode as:

$$\hat{G(s)} = \frac{8.3782 \times 10^6}{s^2 + 57.2s + 6.657 \times 10^6}. \tag{14}$$

Step 1: The inner loop is calculated to use the maximum sensor's bandwidth, which is 5 kHz. Using (6), the resonance-shifting gain is 117. This shifts the system resonance from 411 Hz to 5 kHz.

$$H_1(s) = \frac{9.803 \times 10^8}{s^2 + 57.2s + 9.87 \times 10^8} \tag{15}$$

Step 2: Using Theorem 1, the corresponding IRC gain for maximum damping is 18807, which results in maximum peak to be 5 dB compare to 54.7 dB for $H_1(s)$.

Step 3: A numerical optimization approach is employed to choose the optimal tracking gain. The cost functions are defined as the maximum ± 1 dB bandwidth, and the overall maximum peak less than the damping loop maximum peak (5 dB for this case). Fig 4 shows the maximum bandwidth verses maximum peak. in this case the point of interest should be somewhere less than 5 dB. Considering the restrictions, the selected tracking gain is 7640, resulting in a bandwidth of 3260 Hz and a maximum peak of 2.6 dB.

To ascertain the stability of the overall control scheme, the controllers are simulated on the fourth-order model developed earlier. A comparison between the standard IRC and the resonance-shifting scheme developed herewith is presented in the following section.

V. Comparison between standard and modified IRC

A. Time domain response

Table (I) tabulates the controller parameters for the standard and the resonance-shifting IRC designs. In these cases,

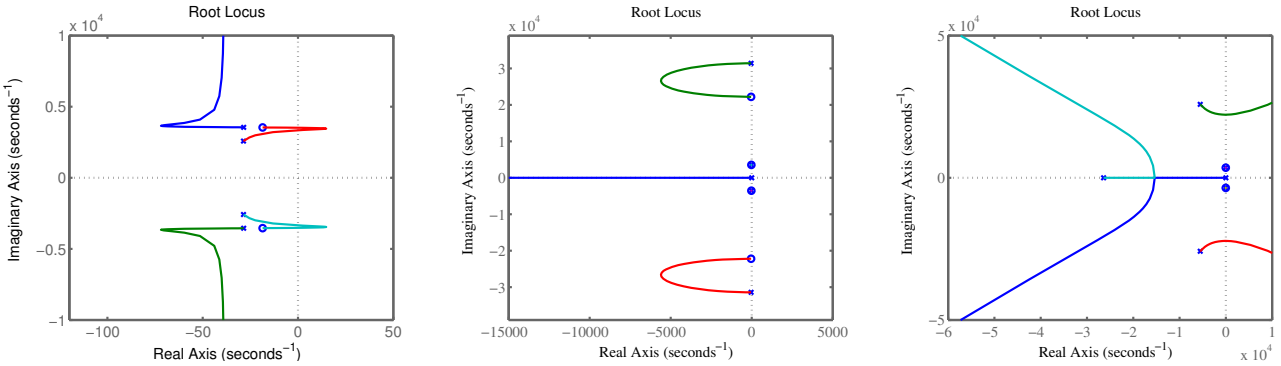

(a) (b) (c)

Fig. 5. (a) Root locus of the resonance shifting loop. The unstable range corresponds to selections of $\hat{k} < 1$ and can easily be avoided. For this simulation, $\hat{k} = 117$ deeming the system stable. (b) shows the IRC damping loop implemented in positive feedback. The lower frequency pair of complex poles moves very close to the complex zeros, thus virtually canceling out their effect. (c) shows the root locus of the damped system in the presence of the tracking controller. The range of k_t to have a stable system is given in Theorem 2.

damping gains are calculated using Theorem 1 to deliver maximum damping and the other parameters are calculated as explained earlier. There is a substantial increase in the positioning bandwidth of the system (by approx. 12 times). The gains of the modified design are significantly higher than the standard IRC. These ranges for gains are implementable and gains as high as 40000 for a standard IRC implementation have recently been reported [8]. Fig. (6) shows the simulation results for the standard and the resonance-shifting IRC for 20 Hz and 250 Hz triangle inputs. Fig. (6)(b) shows the resonance-shifting IRC scheme reduces the time lag between input and output signals. The lag becomes greater when input frequency is increased, Fig. (6)(c).

B. Disturbance rejection

To compare the performance of the standard IRC design with resonance-shifting IRC scheme, the system is exposed to two common types of input disturbances viz: white noise and step signal. Fig. (7)(a) shows the Bode plot of $Y(s)/D_i(s)$ for the standard and resonance-shifting IRC schemes. The resonance-shifting IRC shows a highly improved input disturbance rejection capability compared with standard IRC scheme. Fig. (7)(b) compares the two design where input signal is 20 Hz perfect triangle and white noise disturbance with a power of $10^{-6}\ V^2 s/rad$. Fig. (7)(c) compares two controller output when same input is applied and a 0.1 V step input disturbance applied at $t = 1.04$ s. These time-domain responses further illustrate the improved disturbance rejection offered by the resonance-shifting IRC scheme.

VI. Conclusions

In this work, the IRC scheme is modified to include a resonance shifting control loop that is capable of increasing the positioning bandwidth of any colocated nanopositioner. The modified scheme also possesses excellent input disturbance rejection capability - a key performance criteria for accurate positioning systems. Finally, the effectiveness of the proposed scheme is demonstrated by simulating the resonance-shifting IRC scheme on the model derived from an FRF data set recorded for a commercially available nanopositioner. A twelve-fold increase in positioning bandwidth was achieved. Future work will include experimental verification and bandwidth-dictated parameter optimizations.

References

[1] A. Preumont, *Vibration Control of Active Structures: An Introduction*. Dordrecht: Kluwer, 1997.

[2] D. J. Inman, *Vibration with Control, Measurement, and Stability*. Englewood Cliffs, NJ: Prentice-Hall, 1989.

[3] J. L. Fanson and T. K. Caughey, "Positive position feedback control for large space structures," *AIAA Journal*, vol. 28, no. 4, pp. 717 – 724, 1990.

[4] B. Bhikkaji, M. Ratnam, A. J. Fleming, and S. O. R. Moheimani, "High-performance control of piezoelectric tube scanners," *IEEE Transactions on Control Systems Technology*, vol. 15, no. 5, pp. 853 – 866, September 2007.

[5] H. R. Pota, S. O. R. Moheimani, and M. Smith, "Resonant controllers for smart structures," *Smart Materials and Structures*, vol. 11, pp. 1 – 8, 2002.

[6] S. Salapaka, A. Sebastian, J. P. Clevland, and M. V. Salapaka, "High bandwidth nano-positioner: A robust control approach," *Review of Scientific Instruments*, vol. 73, no. 9, pp. 3232 – 3241, September 2002.

[7] S. S. Aphale, A. J. Fleming, and S. O. R. Moheimani, "Integral resonant control of collocated smart structures," *Smart Materials and Structures*, vol. 16, pp. 439 – 446, February 2007.

[8] Y. K. Yong, B. Bhikkaji, and S. O. R. Moheimani, "Design, modeling, and fpaa-based control of a high-speed atomic force microscope nanopositioner," *IEEE/ASME Transactions on Mechatronics*, 2012, article in Press.

[9] R. L. Clark, "Accounting for out-of-bandwidth modes in the assumed modes approach: implications on collocated output feedback control," *Trans. ASME Journal of Dynamic Systems, Measurement, and Control*, vol. 119, pp. 390 – 395, 1997.

[10] S. S. Aphale, B. Bhikkaji, and S. O. R. Moheimani, "Minimizing scanning errors in piezoelectric stack-actuated nanopositioning platforms," *IEEE Trans. on Nanotechnology*, vol. 7, no. 9, pp. 79 – 90, 2008.

[11] M. Namavar, A. J. Fleming, M. Aleyaasin, K. Nakkeeran, and S. S. Aphale, "An analytical approach to integral resonant control of second-order systems," *IEEE/ASME Transactions on Mechatronics*, (in press), 2013. DOI: 10.1109/TMECH.2013.2253115.

TABLE I

PARAMETERS FOR STANDARD AND MODIFIED IRC

Case	$\hat{k}$	d	k	k_t	Overall Maximum Peak (dB)	Overall Bandwidth (Hz)
Standard IRC	-	-2.52	1220	640	2.12	262
Modified IRC	117	-1.99	18807	7640	2.45	3178

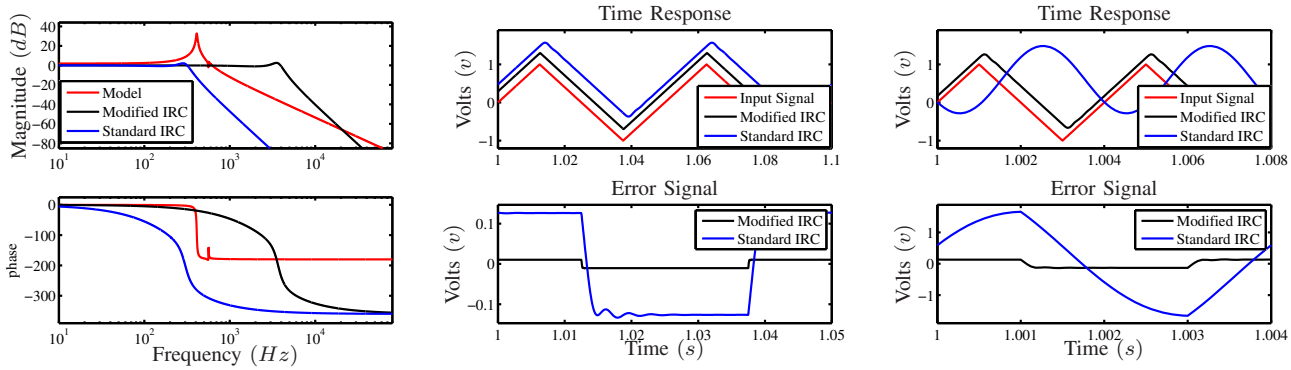

(a) (b) (c)

Fig. 6. (a) Bode plot of the $Y(s)/R(s)$ for fourth order mode, standard and modified IRC. (b) Plot of the output and the error for both designs to 20 Hz triangle wave input. (b) Plot of the output and the error for both designs to 250 Hz triangle wave input. Traces are separated by 0.3 V for clarity.

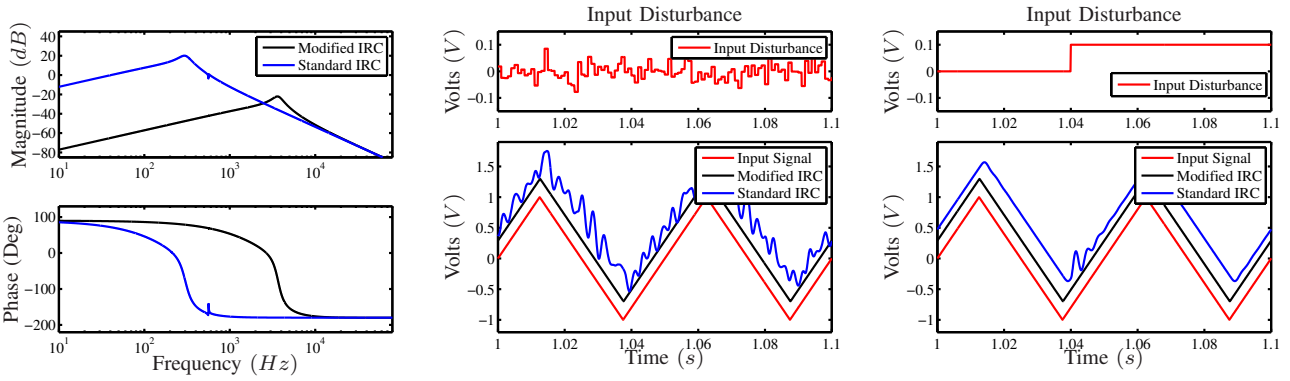

(a) (b) (c)

Fig. 7. (a) shows the Bode plot of $Y(s)/D_i(s)$ for modified and standard IRC. (b) Shows the white noise disturbance and the time trace for the standard and the resonance-shifting IRC schemes. (c) shows the step input disturbance applied at $t = 1.04$ s and the time trace for the standard and the resonance-shifting IRC schemes. For both (b) and (c) the input signal is 20 Hz triangle wave. Traces are separated by 0.3 V for clarity.

[12] A. J. Fleming, S. S. Aphale, and S. O. R. Moheimani, "A new method for robust damping and tracking control of scanning probe microscope positioning stages," *IEEE Transactions on Nanotechnology*, vol. 9, no. 4, pp. 438 – 448, July 2010.

[13] E. Pereira, S. S. Aphale, V. Feliu, and S. O. R. Moheimani, "Integral resonant control for vibration damping and precise tip-positioning of a single-link flexible manipulator," *IEEE / ASME Transactions on Mechatronics*, vol. 16, no. 2, pp. 232 – 240, April 2011.

[14] Y. K. Yong, S. S. Aphale, and S. O. R. Moheimani, "Design, identification, and control of a flexure-based xy stage for fast nanoscale positioning," *IEEE / ASME Transactions on Mechatronics*, vol. 8, no. 1, pp. 46 – 54, January 2009.

[15] B. Basu and S. R. K. Nielsen, "A multi-modal control using a hybrid pole-placementintegral resonant controller (ppir) with experimental investigations," *Structural Control and Health Monitoring*, vol. 18, pp. 191 – 206, 2011.

[16] I. M. Diaz, E. Pereira, and P. Reynolds, "Integral resonant control scheme for cancelling human-induced vibrations in light-weight pedestrian structures," *Structural Control and Health Monitoring.*, p. doi: 10.1002/stc.423, 2011.

[17] S. Devasia, E. Eleftheriou, and S. O. R. Moheimani, "A survey of control issues in nanopositioning," *IEEE Transactions on Control Systems Technology*, vol. 15, no. 4, pp. 689 – 703, July 2007.